Max-Planck-Institut
für Meteorologie

REPORT No. 125

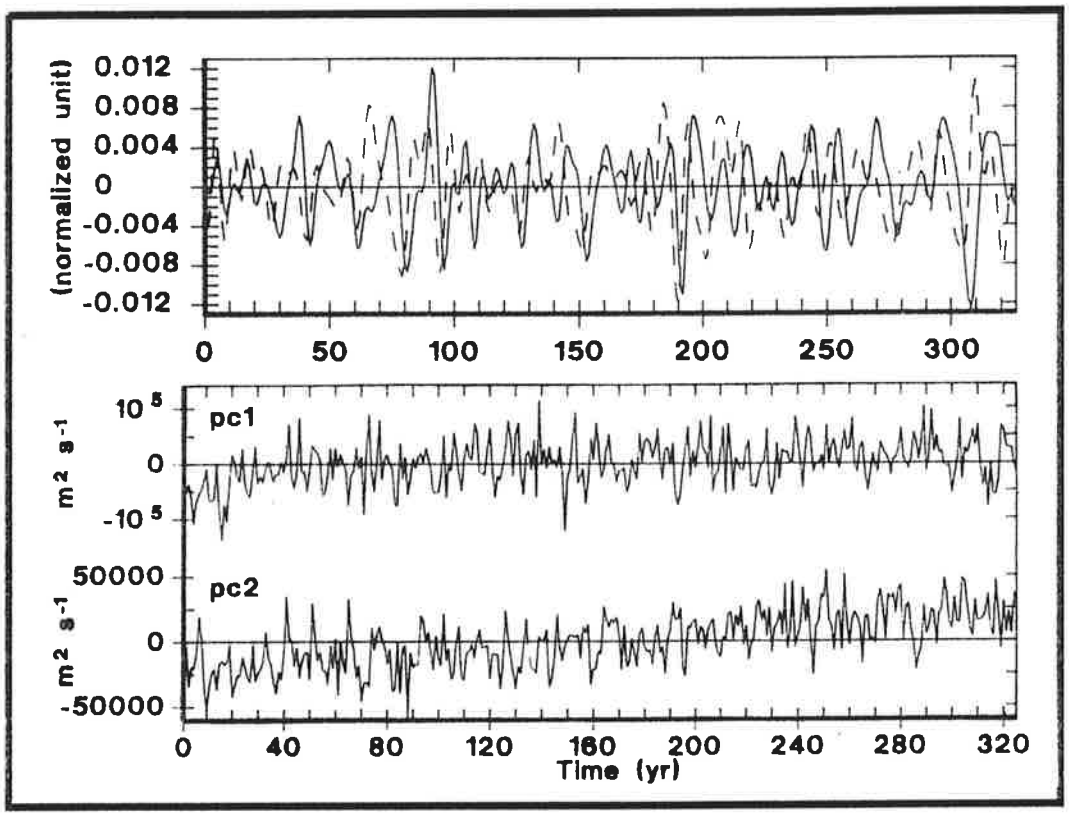

INTERDECADAL VARIABILITY IN A GLOBAL COUPLED MODEL

by

JIN-SONG VON STORCH

HAMBURG, JANUARY 1994

AUTHOR:

Jin-Song von Storch

Max-Planck-Institut
für Meteorologie

MAX-PLANCK-INSTITUT
FÜR METEOROLOGIE
BUNDESSTRASSE 55
D-20146 Hamburg
F.R. GERMANY

Tel.: +49-(0)40-4 11 73-0
Telemail: MPI.METEOROLOGY
Telefax: +49-(0)40-4 11 73-298

Interdecadal variability in a global coupled model

Jin-Song von Storch
Max Planck Institute for Meteorology
Hamburg, Germany

February 4, 1994

Abstract

Interdecadal variations are studied in a 325-year simulation performed by a coupled atmosphere - ocean general circulation model. The patterns obtained in this study may be considered as characteristic patterns for interdecadal variations.

1. The atmosphere: Interdecadal variations have no preferred time scales, but reveal well-organized spatial structures. They appear as two modes, one is related with variations of the tropical easterlies and the other with the Southern Hemisphere westerlies. Both have red spectra. The amplitude of the associated wind anomalies is largest in the upper troposphere. The associated temperature anomalies are in thermal-wind balance with the zonal winds and are out-of-phase between the troposphere and the lower stratosphere.
2. The Pacific Ocean: The dominant mode in the Pacific appears to be wind-driven in the midlatitudes and is related to air-sea interaction processes during one stage of the oscillation in the tropics. Anomalies of this mode propagate westward in the tropics and then northward (southwestward) in the North (South) Pacific on a time scale of about 10 to 20 years.

ISSN 0937–1060

1 Introduction

Decadal time scale changes in the climate system have drawn the increasing attention of researchers. Recently, a decadal time scale change in atmospheric circulation has been identified by Trenberth (1990). He demonstrated that there is an obvious change in the North Pacific sea level pressure during the winter time between 1946-76 and 1977-87. This " climate change" is accompanied by a signal over the North Pacific throughout the troposphere, in the North Pacific sea surface temperature (SST), and probably also in the tropical SST (Nitta and Yamada,1989; Salmon, 1992 and Xu, 1993). Another atmospheric circulation change is noted by Xu (1993). She found that the Southern Hemisphere westerlies become stronger after the mid-seventies in her twenty year data set.

A well-known oceanic interdecadal variation is the "Great Salinity Anomaly" (GSA) which is characterized by a freshening of the surface waters of the North Atlantic during the 1960s and 1970s (Dickson et al., 1988). Interdecadal variations are also found in SST anomalies over different regions.

Following the observational studies, the atmospheric variations on time-scales longer than one year, and the interdecadal variations in the North Atlantic and the North Pacific have been studied using (simplified) uncoupled models (James and James, 1992; Robinson, 1993; Weisse et al., 1993; Delworth et al., 1993; Graham, 1992; Miller et al., 1992). However, some basic questions, such as whether these variations have quasi-periodic character or just fluctuate randomly on time scales of several years, and what the role of the atmosphere (ocean) is for the oceanic (atmospheric) circulation changes, are still not understood. It is also unclear whether a present-day coupled general circulation model (GCM) is able to reproduce the observed decadal time-scale variations.

To answer these questions, the output of a long-term integration performed by a coupled GCM is analyzed. The atmospheric component of the coupled model is the ECHAM-1 T21 model which is the Hamburg version of the ECWMF operational numerical weather prediction model adapted for climate simulation purposes. The horizontal resolution is limited by a triangular spectral cut-off to a total wave number of 21 representing a 64 longitude by 32 latitude grid (Roeckner et al., 1992). The oceanic component is the Hamburg LSG (Large Scale Geostrophic) model which is based on a numerical formulation of the primitive equations for large scale geostrophic motion. The ocean model is based on 11 variably spaced vertical levels and an effective grid-size of 4^o (Maier-Reimer et al., 1993).

Before coupling, the ocean model was integrated for 7000 years in a spin-up run. The first 5000 years of this run was driven by the monthly climatological wind stress fields from Hellerman and Rosenstein (1983), an effective monthly mean air temperature constructed from the COADS (Woodruff et al. 1987) and the annual-mean surface salinity from Levitus(1982). The last 2000 years was driven by the fresh water fluxes which were diagnosed from the first 5000 years, and the same wind stress and air temperature forcings as used before. The final state of this integration

was then coupled to the ECHAM-1 model.

The atmosphere and ocean components are coupled by the air-sea fluxes of momentum, sensible and latent heat, short and long wave radiation and fresh water (Cubasch et al., 1992). To avoid a climate drift of the coupled system, a flux correction (Sausen et al., 1988) is applied. This is equivalent to coupling the atmosphere and ocean with anomalies of the fluxes computed relative to the equilibrium states of the uncoupled sub-systems. The flux correction is designed to ensure that the climatology of the atmospheric component is essentially identical to that of the uncoupled model documented by Boer et al. (1991) and the climatology of the oceanic component is similar to that of the uncoupled model documented by Maier-Reimer et al. (1992). The output analyzed here contains 325 model years from year 9 to 333. The first 100 years of the coupled model simulation have been documented by Cubasch et al. (1992).

The state of the coupled model after 333 years of integration is briefly presented in section 2. Two dominant atmospheric interdecadal modes are shown in section 3. The results suggest that the circulation can vary over several years with no preferred time scale. In section 4, a pronounced interdecadal mode in the Pacific is described. In both section 3 and 4, special attention is paid to the air-sea coupling parameters. A summary is given in section 5.

In the following, unless explicitly noted, monthly data are used for the atmosphere whereas oceanic data are yearly. In section 3 and 4, only anomalies are considered. They are derived by subtracting the 325-year mean annual cycle for the atmospheric data and by subtracting the 325-year mean for the oceanic data.

2 The State of the coupled model

Before analyzing the variability, we summarize a few salient features of the coupled model. The mean fields are averaged over 325 years. Fig.1a and 1b show the zonally-averaged profiles of the zonal wind component in January and July. The secondary wind maximum of the Southern Hemisphere winter-time double-jet is absent, a feature typical of low resolution models (Xu et al. 1990), but the amplitude and the location of the major tropospheric jets are simulated reasonably well. The standard deviation of the zonal mean zonal wind anomalies is shown in Fig.1c. Largest variances are located over the high latitudes and in the upper troposphere.

The 325-year mean and standard deviation of vertically integrated oceanic mass transport streamfunction is shown in Fig.2. The structure and intensity of the circulation are similar to those produced by the uncoupled model (Maier-Reimer et al., 1992). The variance maxima in the southern oceans indicate variations of the Antarctic Circumpolar Current of order of 5 Sv. In the North Pacific and North Atlantic, variance maxima of order of 2 Sv are situated in the centers of the oceans.

The mean state of the zonally averaged meridional overturning circulation (streamfunction) in the Atlantic is shown in Fig.3. The characteristic features of the overturning are an inflow

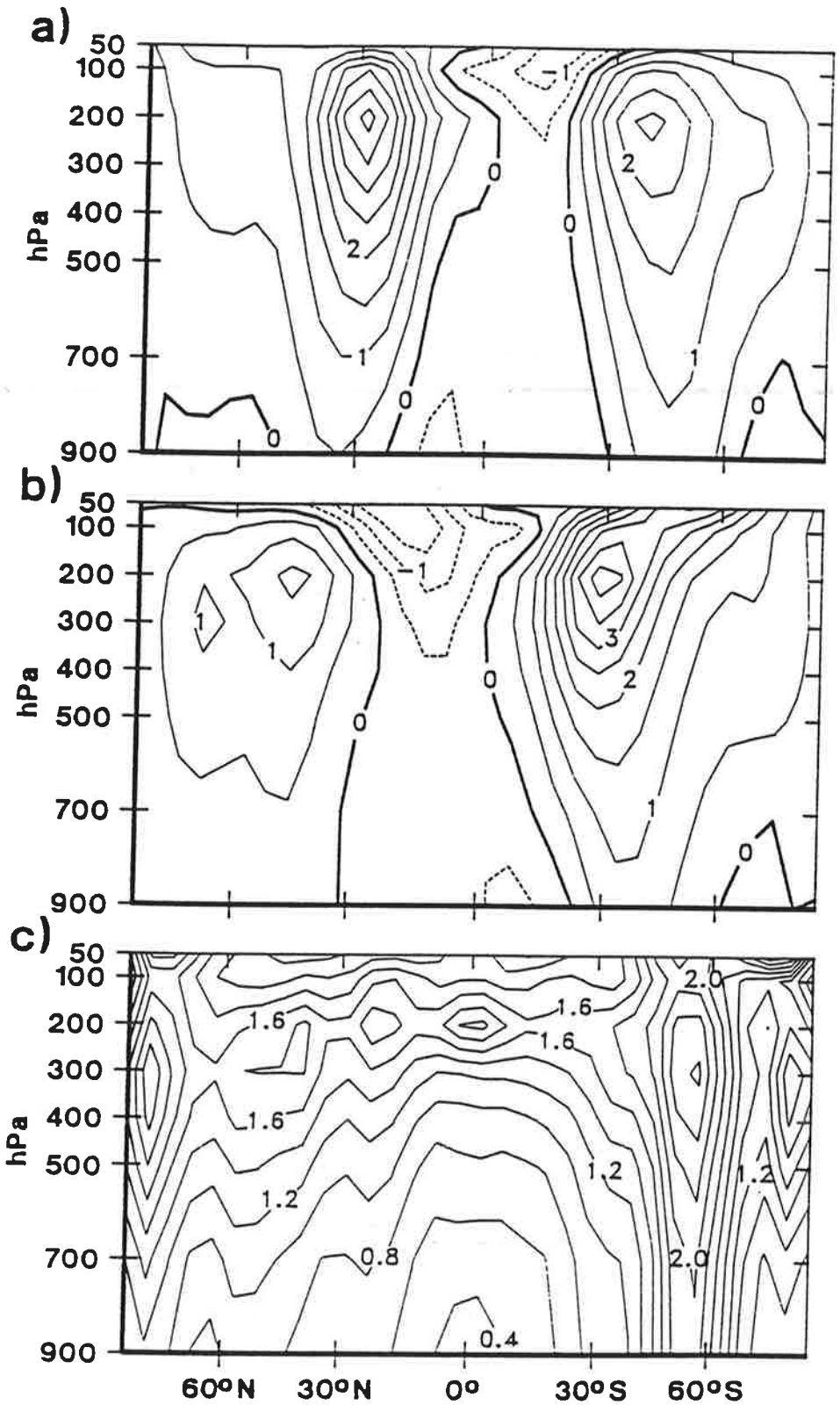

Figure 1: 325-year average of January (a) and July zonal mean zonal wind profiles (10 ms^{-1}) and standard deviation of the monthly zonal mean zonal wind anomalies (c) (ms^{-1}).

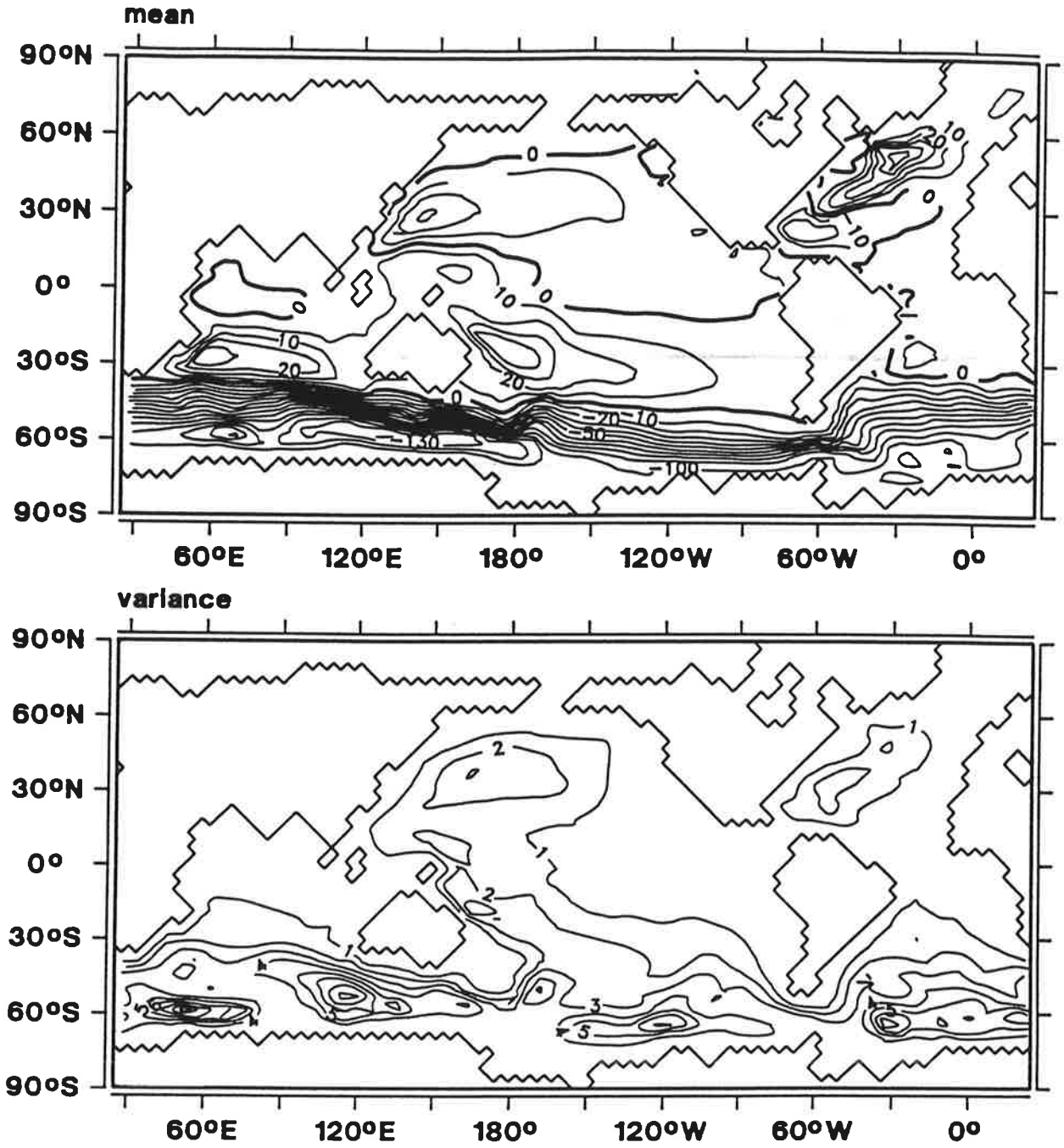

Figure 2: 325-year average of vertically integrated annual-mean mass transport streamfunction (top) and standard deviation of the yearly streamfunction anomalies (bottom). Both in Sv.

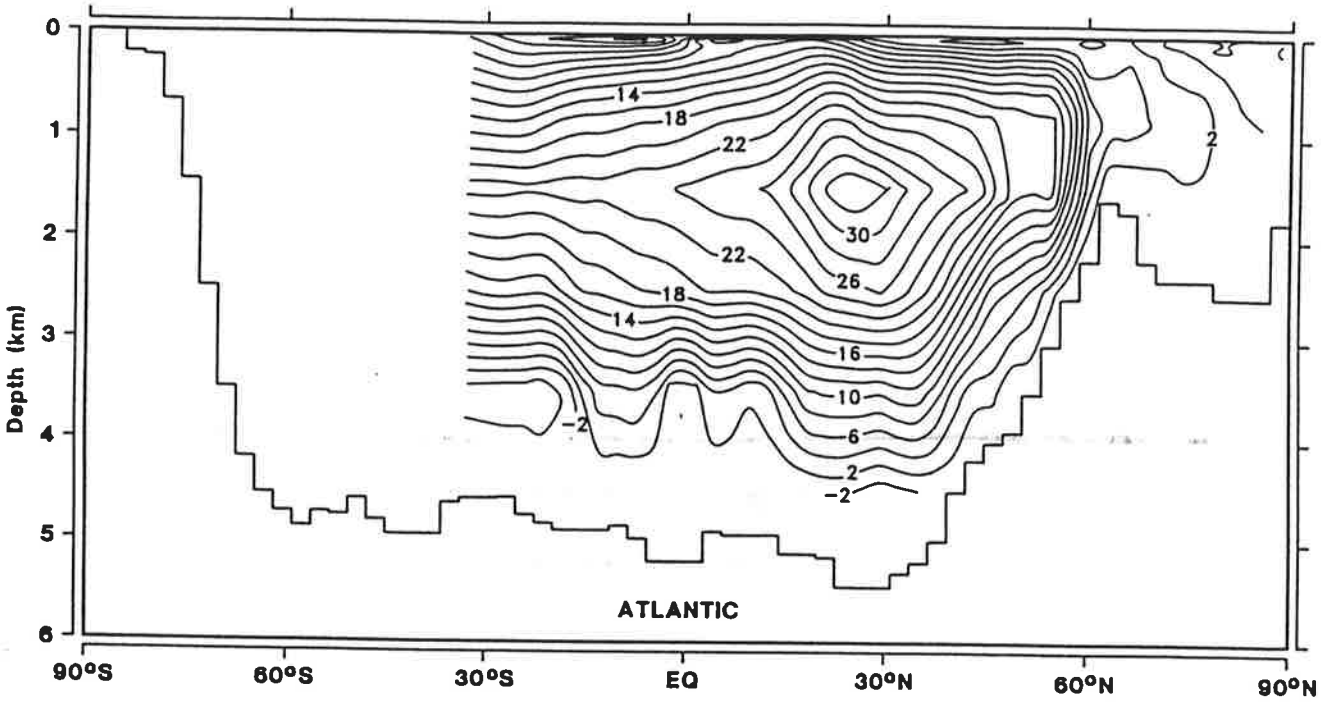

Figure 3: 325-year average of the zonally integrated meridional streamfunction in the Atlantic (Sv).

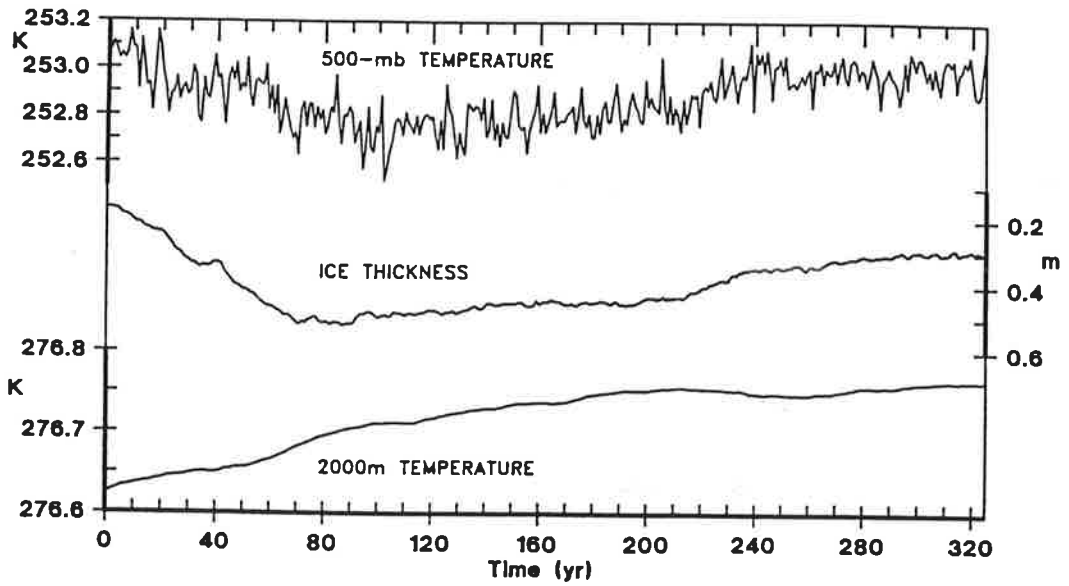

Figure 4: Time series of globally averaged 500-mb temperature (K), ice-thickness (m) and 2000-meter temperature (K). Note that the global average of the ice thickness does not correspond to the mean ice thickness since ice is not a global variable.

of about 12 Sv from the Southern Ocean in the upper kilometer and a strong outflow of about 20 Sv from the North Atlantic and a small bottom inflow from the south. The bottom inflow is weaker in the coupled model than in the uncoupled model (Fig.3b from Maier-Reimer et al., 1992).

Fig.4 shows time series of globally averaged 500-mb temperature, ice thickness and 2000-meter ocean temperature. The atmosphere is quasi-stationary with respect to the global mean 500-mb temperature. A comparison between the time series of 500-mb temperature and ice thickness suggests that the decrease (increase) of the tropospheric temperature in the first 100 (afterward) years is related to the growth (decay) of the global ice volume. The amplitude of the ice-related temperature changes is about 0.5K.

In contrast to the atmosphere, the ocean is not yet in equilibrium. There is a global warming of about 0.1 to 0.2K per 300 years in the model ocean. The warming comes to an end in the upper ocean after 100 years, so that the rise of the thermocline is only visible in the first 100 years. In the Pacific, the surface of $\rho = 26.6 kgm^{-3}$ rises 40 meters within the first 100 years and then stays quasi-stationary. In the deep ocean, however, more time is needed for the ocean to reach a quasi-equilibrium state. In 4000-meter depth, the temperature increases throughout the integration time without any indication of reaching a nearby stationary state.

3 Interdecadal modes in the atmosphere

3.1 Temporal and spatial structures

When we talk about the interdecadal variations in the atmosphere, we are not sure whether these variations vary in a limited frequency band or show up as erratic phenomenon. The latter may appear as sequences of persistent negative (or positive) episodes with variable durations. However, if one has only a short time series, as in the case of Trenberth (1990) and Xu (1993), these temporal behaviors can not be discriminated.

In order to answer this basic question, we assume that the interdecadal variations have large scales and consider first spectra which are obtained by averaging those of the time series at each grid points. The top curve in Fig.5 is such a spectrum averaged for the 200-mb streamfunction. The spectrum consists of two parts. The one on the time scale shorter than 2 years is derived from 10 years of daily anomalies (model year 91 to 100); whereas the other part on the time scale longer than 2 months is derived from 325 years of monthly anomalies. On the overlapping frequencies, the two spectra have the same energy level. The spectrum at each grid point is estimated from five subsequent chunks of the corresponding time series. In general, there is an increase of energy with increasing time scales. The spectrum is red and shows a wide plateau without any pronounced spectral peak on the time scale longer than one year. The spectral maximum at the low-frequency end is related to the trend of the time series (see Fig.7).

The model atmosphere does not prefer any specific frequency on the time scales longer than

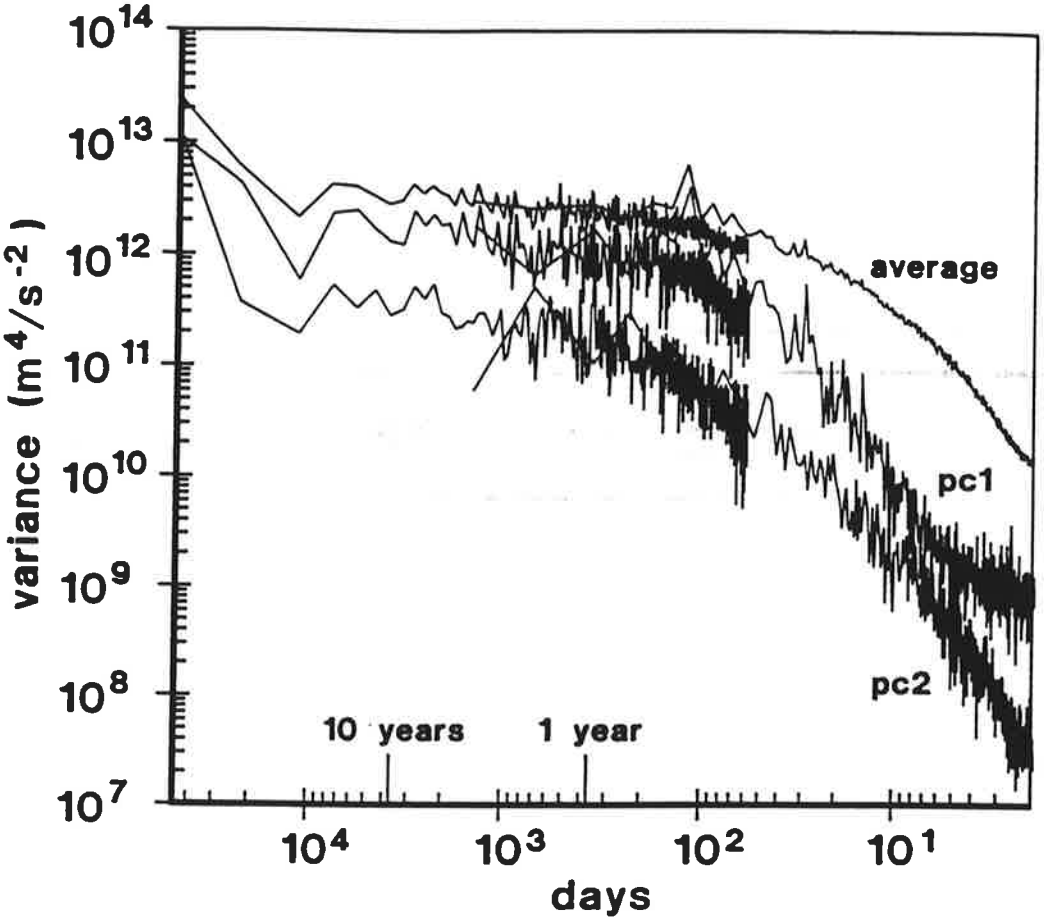

Figure 5: Spectra of 200-mb streamfunction and of PC1 and PC2. All three spectra are derived from averaging those of the time series at each grid point, the top one corresponds to the unfiltered 200-mb streamfunction fields and the other two correspond to fields which are reproduced by multiplying EOF1 (EOF2) with PC1 (PC2).

1 year. Does the atmosphere prefer certain spatial patterns?

Several EOF and POP (see Section 4) analyses were carried out to study the spatial structure of variations on time scales longer than 1 year. The dominant modes reveal standing character and can be described by the leading EOFs. Fig.6 shows EOF1 and EOF2 obtained from filtered data where variations on time scales shorter than 7 and longer than 50 years are suppressed. They explain 63% of the filtered variance. The patterns change very little when different filter windows are used or different levels are chosen (not shown). This fact suggests that EOF1 and EOF2 are the dominant patterns of the atmospheric variations on different time scales.

This suggestion is supported by the spectra of the time series which are obtained by projecting the monthly or daily (only year 91 to 100) unfiltered 200-mb streamfunction data onto EOF1 and EOF2 (Fig.5). The time series are denoted hereafter by PC1 and PC2. Their spectra are averaged over the spectra at i-th grid point $\mathbf{x_i(t)}$ with $\mathbf{x_i(t)} = \alpha(\mathbf{t}) \times \mathbf{p_i}$ where $\alpha(t)$ are daily or monthly PC1 (PC2) and $\mathbf{p_i}$ is the EOF pattern at i-th grid point. Thus, the three spectra in Fig.5 are comparable to each other with the top one including all spatial scales and the lower two only for two specific spatial structures given by EOF1 and EOF2.

The spectra of PC1 and PC2 are much redder than the averaged spectrum. The variance contributed by PC1 or PC2 increases with increasing time scales so that the difference in energy levels between the averaged spectrum and those of PC1 and PC2 is smaller on the low-frequency range than those on the high-frequency range.

The yearly values of PC1 and PC2 are shown in Fig.7. The time series confirm the temporal character indicated by the red spectra in Fig.5. If monthly values are plotted, say for PC2 in the time period from year 155 to year 175, a behavior similar to those described in the observations is found. The atmosphere can stay in the state given by EOF1 or EOF2 over several years and then change to the opposite state and stay there for another few year period.

Back to the spatial structures, Fig.8 shows patterns of zonal mean zonal wind and zonal mean temperature which are related to PC1 and PC2. They are called regression patterns and are calculated by minimizing the following equation:

$$\langle (\mathbf{x}(t) - \frac{\alpha(t)}{\delta}\mathbf{p})^2 \rangle = min \qquad (1)$$

where $\langle\rangle$ indicates expectation, $\alpha(t)$ is PC1 or PC2, δ its standard deviation, $\mathbf{x}(t)$ anomalies of zonal mean zonal wind or zonal mean temperature. As the solution of (1), the regression $\mathbf{p}_i$ at the i-th grid point is simply the correlation between the normalized PC and $\mathbf{x}_i$. The normalization ensures that the values in a regression pattern correspond to one-standard-deviation anomalies in physical units.

Compared with the mean state (Fig.1), EOF1 is associated with changes in the intensity of the tropical easterlies (Fig.8a) and EOF2 with a shift of the Southern Hemispheric jet (Fig.8b). The wind anomalies are in thermal wind balance with the temperature anomalies. Since the winds have their largest amplitude in the upper troposphere, the meridional temperature gradi-

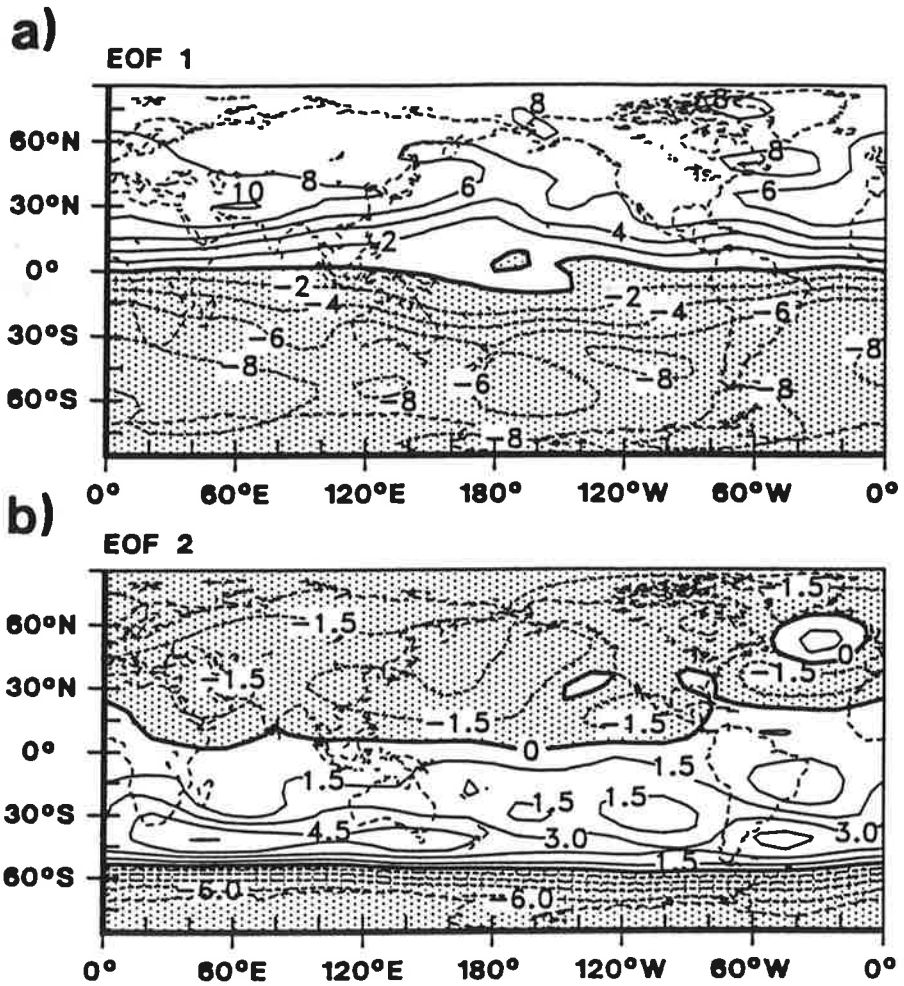

Figure 6: EOF1 and EOF2 calculated from 200-mb streamfunction anomalies. The data are filtered in such a way that variations on time scales shorter than 7 years and longer than 50 years are suppressed.

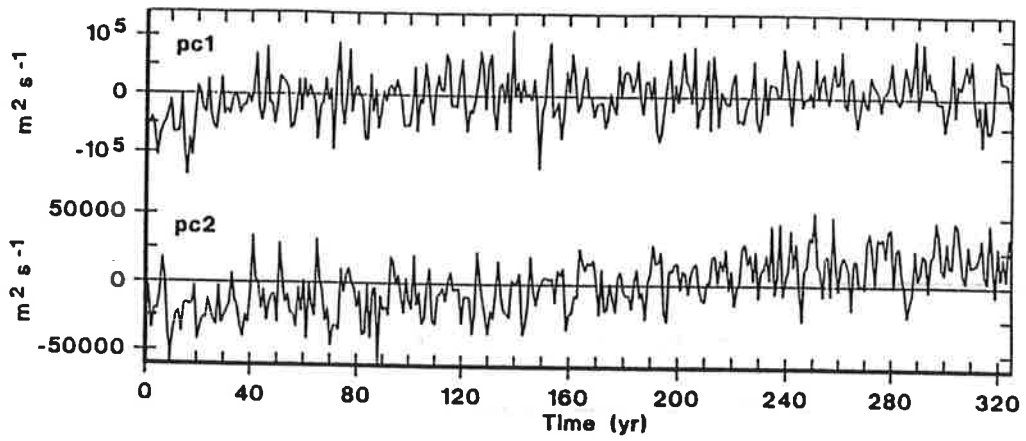

Figure 7: PC1 and PC2 in m^2s^{-1}. They are derived by projecting the unfiltered monthly anomalies onto normalized EOF1 and EOF2 and then taking an average for each year.

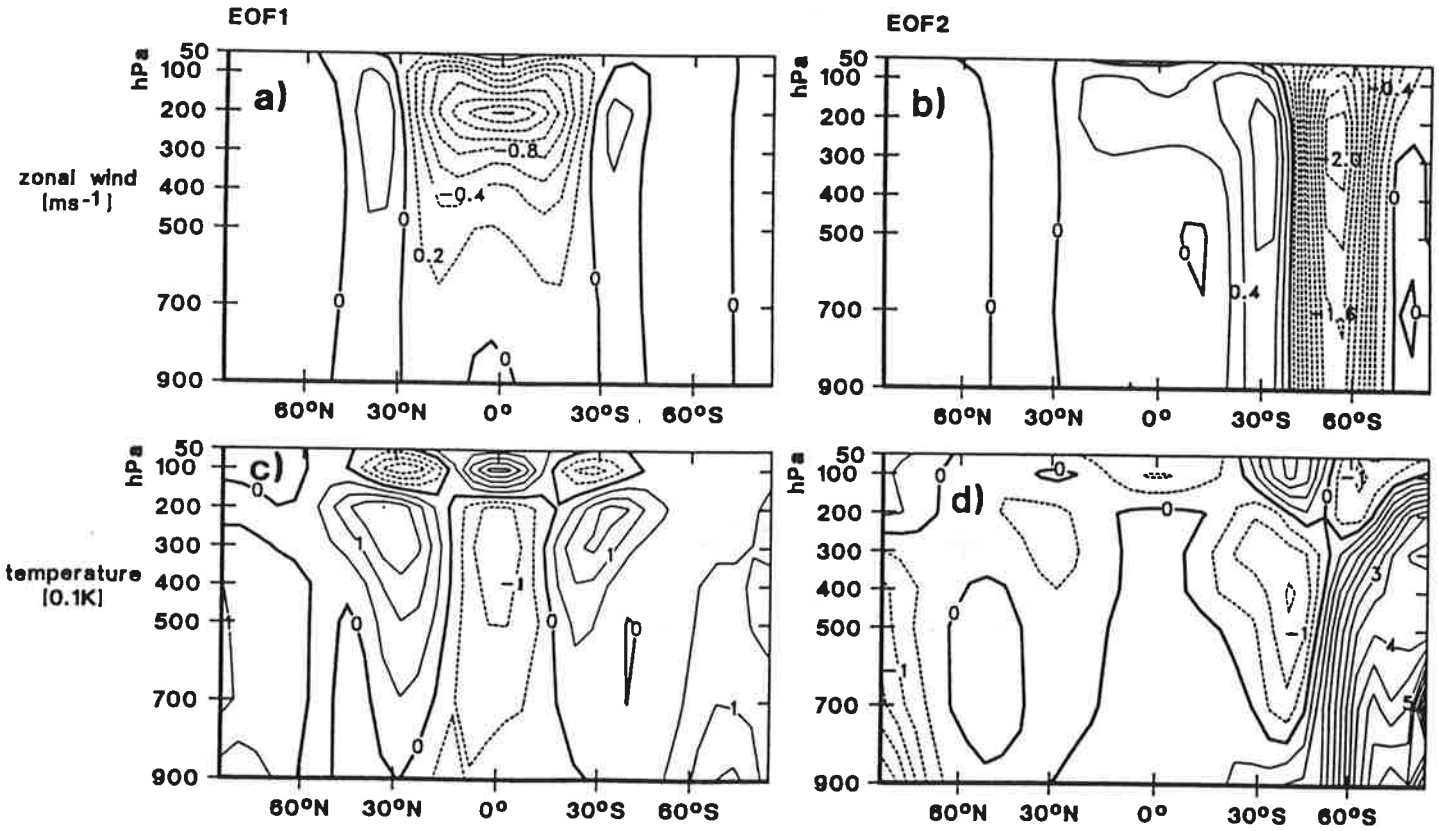

Figure 8: Regression patterns of anomalies of zonal mean zonal winds (ms^{-1}, top) and zonal mean temperature (0.1K, bottom) related to EOF1 (left) and EOF2 (right).

ent changes its sign around the tropopause so that the temperature anomalies in the troposphere are out-of-phase with those in the lower stratosphere (Fig.8c and 8d). In the tropics (over the Southern Ocean), Fig.8a (8b) explains up to 60% of the total unfiltered variance of the zonal mean zonal winds whereas Fig.8c (8d) up to 20 to 30% of the total unfiltered variance of the zonal mean temperature. The one-standard-deviation wind anomalies are of order of 1 to 1.5 ms^{-1} and those of temperature, 0.2 to 0.5K. The amplitude of the temperature anomalies is comparable to the largest variability in the tropospheric temperature changes which are related to the ice variations (Fig.4).

3.2 The role of the ocean

To study the possible role of the ocean in generating the atmospheric modes described in Section 3.1, sensible and latent heat flux anomalies are considered. Apart from radiation, the heat fluxes through the air-sea interface are the only external forcing for the atmosphere, insofar as they depend on external parameters such as SST and sea ice skin temperature.

Two conceptually opposite cases are considered. In the case when atmospheric variations are not generated by the underlying oceans, the heat flux would vary in-phase with the air temperature. Furthermore, the anomalous atmospheric circulation would produce changes in the wind driven circulation of the ocean which would develop mainly parallel to PC1 and PC2.

If the atmospheric variations were entirely generated by the underlying oceans, the corresponding heat flux forcing $f(t)$ would satisfy:

$$\frac{d\alpha(t)}{dt} = f(t)$$

where $\alpha(t)$ indicates PC1 or PC2. That is $f(t)$ would be 90° out-of-phase with $\alpha(t)$ over a wide frequency band. It is assumed that the heat flux forcing displays the same spatial structure on all time scales and its temporal evolution is given by $f(t)$. This assumption is reasonable because the responses which are given by Fig.6 and Fig.8 have the same pattern on different time scales.

Following these notions, the phase relationships between the heat flux and PC are calculated using equation (1) (for the 90° out-of-phase relationship $\alpha(t)$ in (1) is replaced by $f(t)$). The in-phase relationship is weak. The PC1 related regression pattern of latent heat flux explains up to 5% of the total variance in the tropical region and the PC2 related regression pattern of the sensible heat flux explains up to 10% in the southern oceans. But the 90° out-of-phase relationship is even worse. The patterns related to $f(t)$ show a patchy structure and explain no variance at all.

Indeed all oceanic changes which are associated with PC1 or PC2 may be understood as changes induced by anomalous wind forcing. The EOF1 related negative SST anomalies (the top diagram of Fig.9) appear together with well organized easterly wind stress anomalies and anomalous upwelling in the tropics whereas the EOF2 related positive SST anomalies in the Southern

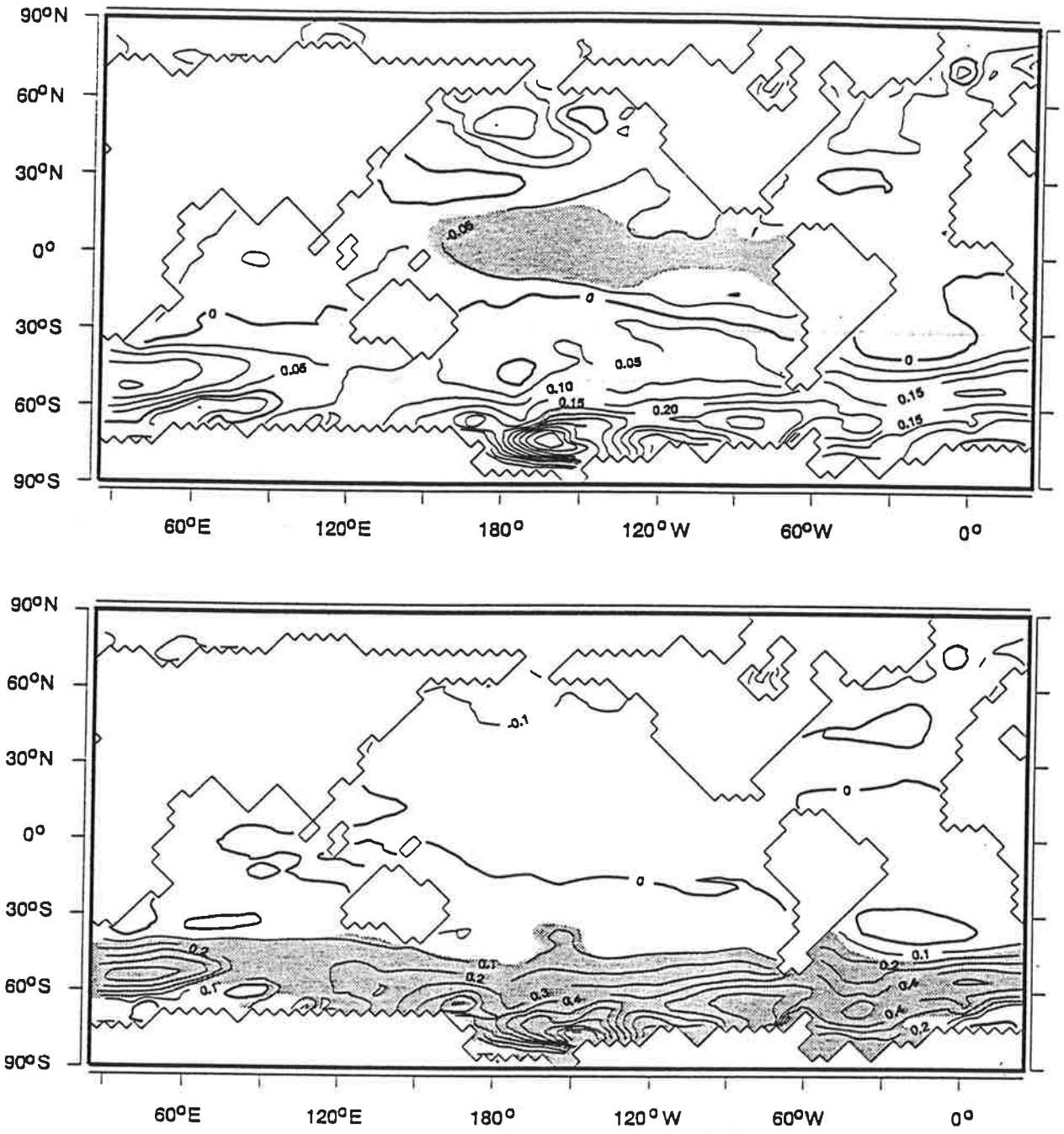

Figure 9: Oceanic surface temperature anomalies related to EOF1 (top) and EOF2 (bottom) in K. The shaded areas indicate regions where the variance explained by the corresponding regression pattern is larger than 10%.

Ocean (the bottom diagram of Fig.9) appear together with easterly wind stress anomalies over the Southern Ocean which cause weaker Antarctic Circumpolar Current, and an anomalous southward Ekman transport and anomalous downwelling north of the Antarctic (not shown).

4 An Interdecadal mode in the Pacific Ocean

This paper considers only interdecadal variations in the Pacific region. In contrast to the atmosphere, oceanic variations display propagating features. The Principal Oscillation Pattern (POP) analysis (Hasselmann, 1988 and H. von Storch et al., 1988) is applied to the Pacific sea level data in order to identify the temporal and spatial characteristics of these variations. Because of the trend in temperature and salinity (section 2) which is also reflected in the surface elevation, only filtered sea level time series are used where variability on time scales shorter than four years and longer than sixty years is suppressed. The same filter is applied to all other parameters which are considered in this section.

The POP analysis assumes that the multivariate time series can be described by a first-order multivariate autoregressive process. The system matrix **A** of this process is estimated from the lag-1 and lag-0 covariance matrix of the considered time series. The eigenvalue of **A** indicates the frequency with which the corresponding eigenvectors (which are called POPs) oscillate. In the case of complex POPs, the coefficient time series of the real and imaginary part of the eigenvector are 90° out-of-phase and oscillate coherently with the frequency given by the eigenvalue. The corresponding POP patterns follow each other on time intervals of about one quarter of a period and describe the spatial evolution of the signal.

4.1 Temporal and spatial structure

One dominant mode which appears as a complex POP is found in the Pacific sea level. Fig.10 shows the coefficient time series. The dashed line in Fig.10 leads the solid line by about 90^0. This implies that the pattern associated with the dashed line (Fig.11a) appears about a quarter of an oscillation period earlier than that associated with the solid line (Fig.11b). The oscillation period, as derived from the POP analysis, is 17 years. The mode, as monitored by the POP coefficient time series (Fig.10), is more intense in the model years from 70 to 100 and around model years 190 and 310.

The first POP pattern (Fig.11a) is characterized by positive sea level anomalies in the tropical central and eastern Pacific and negative anomalies northwest and southwest of these. After a quarter of a period, the tropical anomalies have moved westward and appear more pronounced north of the Equator (Fig.11b), while negative anomalies have propagated northward in the North Pacific and southwestward in the South Pacific. The time interval which is needed for anomalies to occur and to cross the subtropical Pacific is about 4 to 5 years.

Amplitudes of the associated sea level anomalies can be derived by multiplying the POP

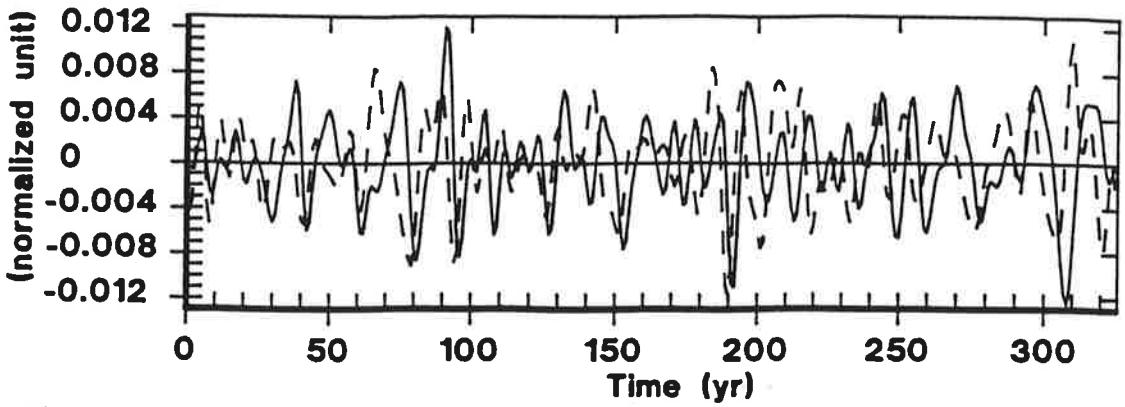

Figure 10: Coefficient time series of the Pacific mode as derived from a POP analysis for sea level anomalies.

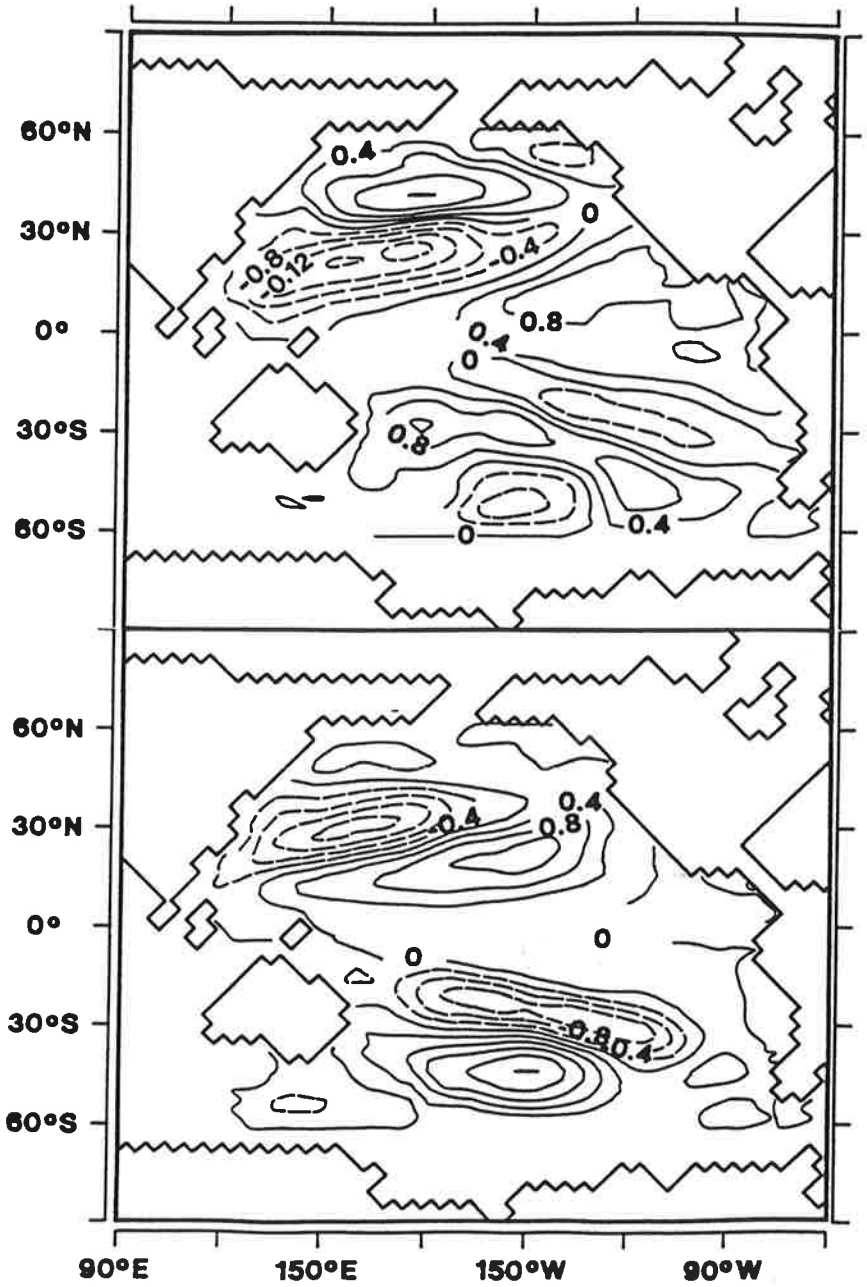

Figure 11: Characteristic patterns of the Pacific mode as derived from a POP analysis for sea level anomalies. The upper diagram appears about one quarter of a period earlier than the lower diagram.

patterns (Fig.11) with their coefficient time series (Fig.10) which gives sea level anomalies of about 0.5 to 1 cm. The Pacific mode explains up to 35% of the total filtered variance. The northern part of the mode is more pronounced than the southern part.

The Pacific mode is not only reflected in sea level but also in other parameters. The 3-dimensional structure is again studied by means of regression patterns. In this case, the equation to be minimized is:

$$\langle(\mathbf{x}(t) - \frac{z_r(t)}{\delta_r}\mathbf{p_r} - \frac{z_i(t)}{\delta_i}\mathbf{p_i})^2\rangle = min \qquad (2)$$

where $\mathbf{x}(t)$ is anomalies of the considered parameter, $z_r(t)$ and $z_i(t)$ are the coefficient time series of the real and imaginary part of the complex POP with standard deviations denoted by δ_r and δ_i (Fig.10), and $\mathbf{p_r}$ and $\mathbf{p_i}$ the regression patterns of this parameter. The parameters are filtered in the same way as for sea level. The regression patterns and POP patterns display the same temporal evolution as that indicated by the POP coefficient time series and give a complex description of the mode.

According to the regression patterns, the Pacific mode is related to changes of the current and of the thermal structure. In the upper ocean, the current changes are in geostrophic balance with the the sea level anomalies. Fig.12 shows the patterns of 150-meter current anomalies.

The changes in the vertical thermal structure are shown by regression patterns of temperature anomalies in a vertical cross-section along about 15°N (Fig.13). The positive (negative) sea level anomalies in the subtropical eastern (western) Pacific (Fig.11a) are accomplished by sinking (lifting) of isotherms in the same region (Fig.13a). After a quarter of a period, the isotherms deepen in the upper few hundred meters across almost the entire Pacific along 15°N (Fig.13b) as the positive sea level anomalies move into the central Pacific in Fig.11b. Thus, parallel to the evolution of the sea level anomalies, temperature anomalies move also westward with the largest anomalies located at 150 to 250 meters depth in the west and at 75 to 150 meters in the east. Below 700 meters, both the anomalies and the explained variances (not shown) vanish.

In order to understand the influences of these temperature anomalies on the mean thermal structure, the 325-year annual-mean temperature profile in the model has been considered (not shown). Along 15°N, three distinct regions with a different vertical temperature gradient are found. The upper region which can be considered as the model mixed layer and the lower region which represents the model deep ocean are well separated by a region at about 150 to 700 meters with a sharp vertical temperature gradient. This middle region can be considered as the model thermocline. Thus, the temperature anomalies shown in Fig.13 indicate that the Pacific mode most strongly influences the regions which separate the mixed layer from the thermocline and does not influence the thermal structure below the thermocline.

The vertical structure of the temperature anomalies and the time interval which is needed for sea level anomalies to cross the subtropical Pacific indicate the active role of the first baroclinic Rossby waves in the evolution of the Pacific mode. The unusual part of the evolution, however,

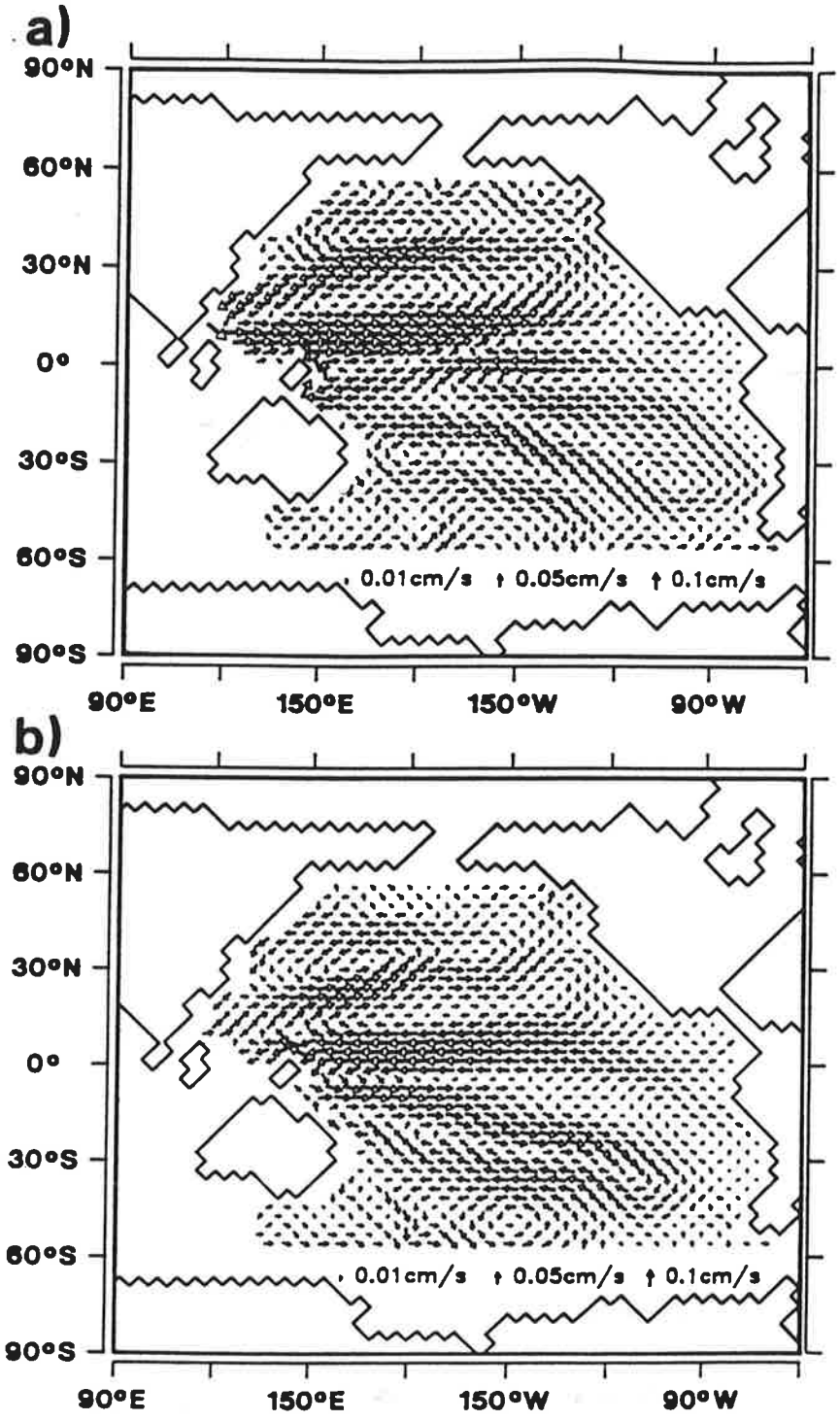

Figure 12: Characteristic patterns of the Pacific mode found in 150-meter velocity (cm/s). They have the same temporary evolution as those indicated by the POP coefficient time series.

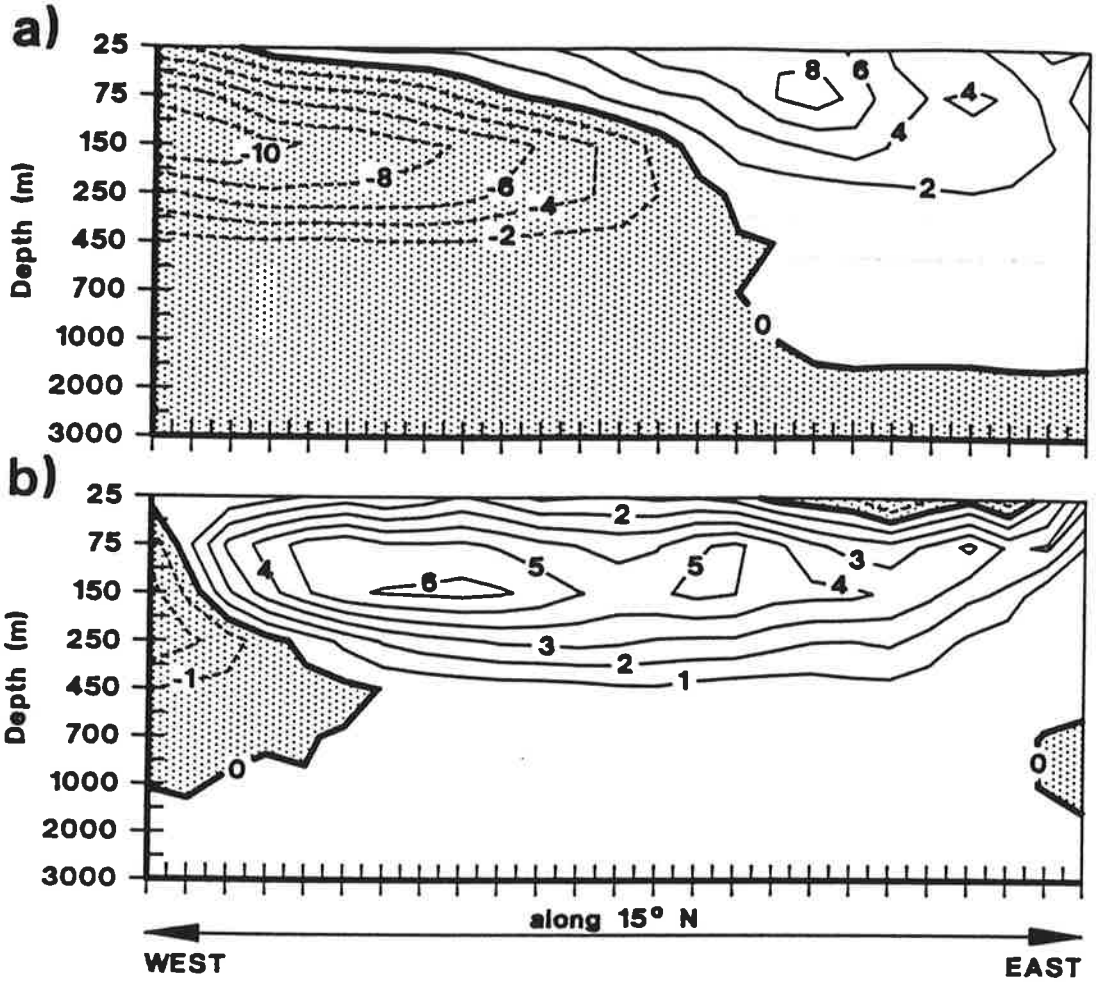

Figure 13: Characteristic temperature patterns of the Pacific mode found in a longitude - height cross-section along 15°N (K). They have the same temporary evolution as those indicated by the POP coefficient time series.

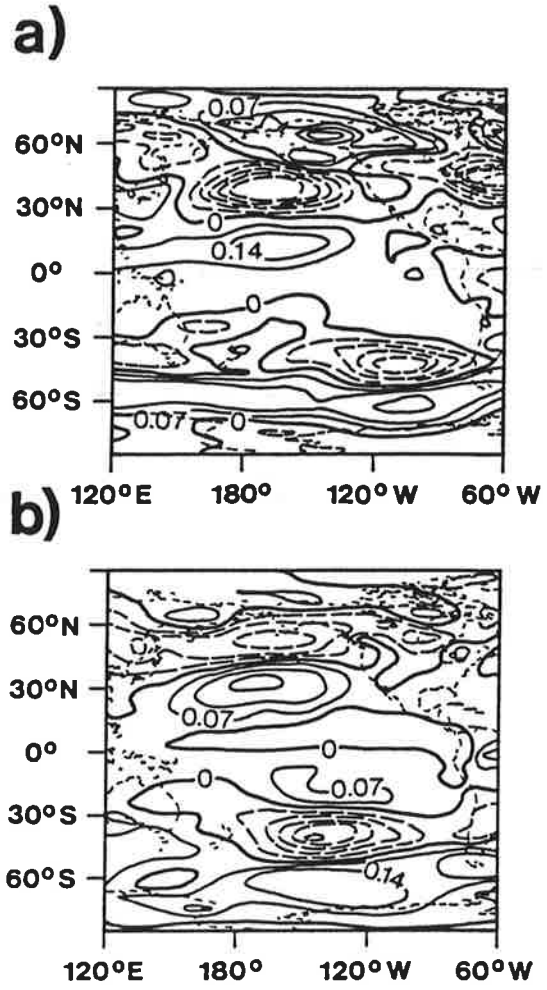

Figure 14: Zonal wind stress patterns which are related to the Pacific mode. They have the same temporary evolution as those indicated by the POP coefficient time series (Pa).

is the subsequent northward (southwestward) propagation in the North (South) Pacific.

4.2 The atmospheric forcing

Regression patterns have been calculated for wind stress, heat flux and freshwater flux. Atmospheric anomalies are averaged for each year since only yearly sea level data are used.

Fig.14 shows regression patterns for zonal wind stress. In the midlatitudes, anomalies of the zonal wind stress (Fig.14) and the current (Fig.12) are in Sverdrup relation, that is that the maxima of the positive (negative) wind stress curl coincide with northward (southward) current anomalies. Towards the tropics, the relationship between the wind stress and the current is only notable in one stage of the cyclic evolution of the Pacific mode, namely the stage described by Fig.12a where the eastward current anomalies along about 15°N are associated with westerly anomalies over the same area in Fig.14a. In the other stage which appears after a quarter of period (Fig.11b, 12b, 14b), the large anomalous westward current in the tropical Pacific is accompanied by very weak wind anomalies.

Regression patterns for the heat flux anomalies suggest that there is an exchange of heat flux between the atmosphere and the ocean in the tropical and the North Pacific regions, especially during the stage described by Fig.11a (not shown). This is the stage when the positive SST anomalies in the central and eastern Pacific (not shown) appear together with the westerly wind stress anomalies in the tropical Pacific. Such a relationship indicates the active role of the tropical air-sea interaction processes.

The Pacific mode found in the coupled model resembles in many respects the observed climate changes during the mid-seventies in and over the North Pacific. This paper suggests that the tropical interaction process plays the important role in one stage of the oscillation. However, further analysis is needed in order to clarify the role of the air-sea interactions in generating this mode.

5 Conclusions

Using a 325-year simulation with the Hamburg ECHAM/LSG model, characteristics of the interdecadal variability are identified. Although some of these features resemble evidence which is obtained from short observational records, the overall picture of the interdecadal variations is new.

There are two dominant interdecadal atmospheric modes, one in the tropics and the other in the Southern Hemisphere. Both display the following characteristic features:

- *No preferred time scales* - The spectra of the corresponding time series are red.
- *Zonal scale* - zonal wave number zero structure.

- *Vertical scale* - throughout the atmosphere with largest anomalies in the upper troposphere.
- *Temperature structure* - troposphere out-of-phase with the lower stratosphere.
- *Amplitude* - Up to 1 - 1.5 ms^{-1} for the zonal mean zonal wind and about 0.2K for the zonally averaged temperature.
- *The role of the ocean* - The lagged relationship between heat flux anomalies suggest that the low-frequency atmospheric variations are not generated by the oceanic anomalies. The related oceanic changes appear to be wind-driven.

The passive role of the ocean in generating atmospheric variations is consistent with the results of James and James (1992) and Robinson (1993) who were able to generate low-frequency variations similar to EOF1 and EOF2 by using a simplified atmospheric model without an oceanic component.

The coupled model generates a dominant interdecadal mode in the Pacific which reveals the following features:

- *Oscillation period of about 17 years.* The intensity of the oscillation, however, shows irregularity.
- *Spatial and vertical scales.* The horizontal scale of the Pacific mode is basinwide. In the vertical direction, temperature anomalies have their largest values near regions which separate the mixed layer from the thermocline and vanish in the deep ocean.
- *Propagation within the basin.* The Pacific mode appears to circulate within the North and South Pacific with the movement of anomalies westward in the tropics, northward in the North Pacific, and southwestward in the South Pacific.
- *Atmospheric forcings.* In the midlatitude regions, wind stress forcings are identified; whereas in the tropics, air-sea interaction processes play active role in one stage of the oscillation.

The overall features of the interdecadal variations in the coupled ECHAM/LSG model are consistent with the observational evidence. The main finding which can not be derived from the observations is the long-term temporal behavior of these modes. For the atmosphere, variations appear as if they were created by a random process with long memory. They are characterized by red spectra. On the other hand, the dominant mode in the Pacific oscillates on time scales of about 10 to 20 years and is characterized by the propagation within the Pacific Basin.

This paper is only a first description of the low-frequency variations generated by a present-day coupled GCM. Further detailed analyses are needed to investigate the origin of these variations.

ACKNOWLEDGMENTS

I express my gratitude to Ulrich Cubasch, Eduardo Zorita, Gabi Hegerl and Dierk Schriever who supported me with the coupled model simulations. Thanks to Claude Frankignoul for his valuable comments as reviewer, and to Ernst Maier-Reimer and Hans von Storch for their help in diagnosing the state of the model ocean and in formulating the results, and to Peter Müller and Gary Michtum for interesting discussions during my stay in their institute. Thanks also to Heinke Höck for assisting me with ocean model post processing, Reiner Schnur and Gabi Hegerl for helping me with the English and Marion Grunnert for preparing the diagrams.

REFERENCES

Boer, G.J.; K. Arpe; M. Blackdurn; M. Deque; W.L. Gates; T.L. Hart; H. Le Treut; E. Roeckner; D.A. Sheinin; I. Simmonds; RNB Smith; T. Tokioka; R.T. Wetherald and D. Williamson; 1990: An intercomparison of the climates simulated by 14 atmospheric general circulation models. - WMO/TD-No 425, Geneva.

Cubasch, U.; K. Hasselmann; H. Höck; E. Maier-Reimer; U. Mikolajewiez; B.D. Santer and R. Sausen; 1992: Time-dependent greenhouse warming computations with a coupled ocean-atmosphere model. - Climate Dyn., **8**, 55-69.

Delworth, T.; S. Manabe and R.J. Stouffer; 1993: Interdecadal variability of the thermohaline circulation in a coupled ocean-atmosphere model. - J. Climate, **6**, 1993-2011.

Dickson, R.R.; J. Meincke; S.A. Malmberg and A.J. Lee; 1988: The "Great Salinity Anomaly" in the northern North Atlantic 1968-1982. - Prog. Oceanogr., **20**, 103-151.

Graham, N.E.; 1993: Decadal-scale climate variability in the 1970's and 1980's: observations and model results. - submitted to Clim. Dyn.

Hasselmann, K.; 1988: PIPs and POPs: The reduction of complex dynamical systems using principal interaction and oscillation patterns. - J. Geophys. Res., **93**, 11015 - 11021.

Hellerman, S. and M. Rosenstein; 1983: Normal monthly wind stress over the World Ocean with error estimates. - J. Phys.Oceanogr., **13**, 1093-1104.

James, I.N. and P.M. James; 1992: Spatial structure of ultra-low-frequency variability of the flow in a simple atmospheric circulation model. - Q. J. Roy. Met. Soc., **118**, 1211-1233.

Levitus, S.; 1982: Climatology atlas of the world ocean. - NOAA Professional Paper 13, 173 pp.

Maier-Reimer, E.; U. Mikolajewicz and K. Hasselmann; 1993: Mean circulation of the Hamburg LSG OGCM and its sensitivity to the thermohaline surface forcing. - J. Phy. Ocean., **23**, 731-757.

Miller, A.J.; D.R. Cayan; T.P. Barnett; N.E. Graham and J.M. Oberhuber; 1993: Interdecadal variability of the Pacific Ocean: Model response to observed heat flux and wind stress anomalies. - submitted to Climate Dynamics.

Nitta, T and Yamada, S.; 1989: Recent warming of tropical sea surface temperature and its relationship to the Northern Hemisphere circulation. - J. Met. Soc. Japan **67** 375 - 383.

Roeckner, E.; K. Arpe; L. Bengsson; S. Brinkop; L. Duemenil; M. Esch; E. Kirk; F. Lunkeit; M. Ponater; B. Rockel; R. Sausen; U. Schlese; S. Schubert and M. Windelband; 1992: Simulation of the present-day climate with the ECHAM model: impact of model physics and resolution. - MPI-report 93.

Robinson, W; 1993: The generation of ultralow-frequency variations in a simple global model. - J. Atm. Sci. **50**, 137-143.

Salmon, D.; 1992: On interannual variability and climate change in the North Pacific. - Ph.D thesis. University of Alaska.

Sausen, R.; K. Barthel and K. Hasselmann; 1988: Coupled ocean-atmosphere models with flux corrections. - Clim. Dyn. **2**, 154-163.

Trenberth, K. E.; 1990: Recent observed interdecadal climate changes in the Northern Hemisphere. - Bull. Am. Meteor. **71** 988 - 993.

von Storch, H.; T. Bruns; I. Fischer-Bruns and K. Hasselmann, 1988: Principal oscillation pattern analysis of the 30 to 60 day oscillation in a GCM. - J. Geophys. Res. **93**, 11022 - 11036.

Weisse, R.; U. Mikolajewicz and E. Maier-Reimer; 1994: Decadal variability of the North Atlantic in an ocean general circulation model. - J. Geophys. Res. In press.

Woodruff, S.; R.J. Sultz; R.L. Jenne and P.M. Steurer; 1987: A comprehensive ocean-atmosphere dataset. - Bull. Amer. Meteor. Soc., **68**, 1239-1250.

Xu, J.S.; H. von Storch and H. van Loon; 1990: The performance of four spectral GCMs in the Southern Hemisphere: the January and July climatology and the semiannual wave. - J. Climate, **3** 53-70.

Xu, J.S.; 1993: The joint modes of the coupled atmosphere-ocean system observed from 1967 to 1986. - J. Climate, **6** 816 - 838.